Finite bending of non-slender beams and the limitations of the *Elastica* theory

Federico Oyedeji Falope[a,b,*], Luca Lanzoni[a,b], Angelo Marcello Tarantino[a,b]

[a] *University of Modena and Reggio Emilia, Department of Engineering Enzo Ferrari, Via P. Vivarelli 10, 41125, Modena, Italy*
[b] *CRICT - Centro Interdipartimentale di Ricerca e per i Servizi nel Settore delle Costruzioni, via P. Vivarelli 10, Modena, 41125, Italy*

Abstract

The problem of slender solids under finite bending has been addressed recently in [**?**]. Here, such a model is extended to short solids by improving the background formulation. In particular, the model is refined by imposing the vanishing of the axial force over the cross sections. The geometrical *neutral loci*, corresponding to unstretched and unstressed surfaces, are provided in a closed form for compressible hyperelastic materials under finite bending. The relevance of the unstressed fibre associated to a nonlinear constitutive law is discussed. It is shown that, in case of non-linear constitutive law as the deformation increases, if the kinematic and mechanical models do not account for the motion of the neutral fibre within the height of the cross section a residual and important axial stress resultant can arise despite of pure bending conditions.

For a generic form of compressible stored energy function, a nonlinear moment-curvature relation accounting for both material and geometric nonlinearities is provided. Such a relation is specialized for a compressible Mooney-Rivlin material. The obtained results are compared with 3D finite element simulations providing excellent agreement. The normalisation of the moment-curvature relation gives dimensionless bending moment as a function of the *Eulerian slenderness* of the solid. This dimensionless plot is able to predict the limitation of

*Corresponding author
Email address: federicooyedeji.falope@unimore.it (Federico Oyedeji Falope)

the *Elastica* arising in case of large deformation of also slender solids. Once the constitutive parameter are fixed, the nonlinear dimensionless bending moment vs Eulerian slenderness curve is valid for any aspect ratio of the bent solid. Such a consideration is valid under the limits of the present theory provided in terms of limits bound of Eulerian slenderness and compactness index.
Keywords: Pure bending, moment-curvature relation, finite elasticity, *Elastica* theory, neutral loci.

---

1. Introduction

The theory of finite bending plays a basic role in various everyday applications. The mechanical response of a variety of structures can be assessed through theory of bending as electro-mechanical components [**?** **?**], biological tissues [**?**], or plants and animals [**?**]. Nonetheless, the well known classical linearised bending theory for beams and plates turns out to be inadequate to provide precise and accurate predictions of strain and stress fields of systems subjected to large bending. This occurs even more for cases where materials exhibit strong geometric or constitutive nonlinearities. For this reason, when linearised theory is inadequate, deformations and stresses of solids are investigated using the *Euler's Elastica* (EE) theory or finite elasticity.

In the framework of linearised elasticity, known as context of small displacements and infinitesimal deformations, the theory of bending was handled in the pioneering works by Bernoulli [**?** **?**], Euler [**?** **?** **?**], and Navier [**?** **?**]. Despite the small deformations, there are many cases in which the constitutive nonlinearities play a pivotal role, as in the cases of plasticity, viscoelasticity or phase changes of the material, in which the constitutive linear bond must be abandoned. For such cases, multi-linear [**?** **?**] or more complex [**?**] constitutive models may be used.

Conversely, where the systems subjected to bending are characterised by large displacements but small deformations, the context of *Euler Elastica* (EE) or simply *Elastica* is more suitable than the linearised elasticity. For such for-

mulation, a linear elastic constitutive law is usually assumed. This is because the EE formulation aims to grasp global aspects as stress resultants distributions or displacements [**?** **?** **?**], contact interaction [**?**] or lose of stability [**?** **?**] problems. Less common are studies in which the EE formulation is coupled to a nonlinear constitutive model integrated with a proper kinematic of the entire cross section of the investigated solid. In the present work the EE formulation combined with a nonlinear constitutive model and associated with the kinematics of the cross section will be called *nonlinear Euler Elastica* (NEE) formulation. A noteworthy approach to investigate systems under large displacements consists in the use of elastic elements, modelled with EE formulation, combined with lumped elasticity element[**?**], translational or rotational springs. However, many authors [**?** **?** **?**] observe that in literature there is a lack of kinematic models to properly couple the transversal behaviour of the cross section with the longitudinal behaviour of a solid. Most of the existing theoretical models models assume a plane strain of stress conditions. Noteworthy is the approach used in [**?**], in which the authors, in order to consider both longitudinal and transversal deformation of a bent solid made of Silicon material, couple the longitudinal finite bending with transversal kinematic based on linearised theory of plates.

The context of finite elasticity (fully nonlinear) removes any assumption on the smallness of the displacements and deformations, and linear constitutive law. Theory of bending was extended to the framework of finite deformations by Rivlin [**?**] using plain strain assumption. Based on the Rivlin work, over time many models have been proposed in the Literature to date. Finite bending of a rectangular block made of Hencky material was investigated in [**?**], whereas in [**?**] finite bending of rectangular block was extended to a general hyperelastic incompressible material. Effect of the electric voltage in a layered elastomer actuator was investigated in [**?**] in terms of plane deformation in the context of electroelasticity. For a wide class of store energy functions, the problem of bending has been addressed in [**?**] investigating the of nonlinearities on the moment curvature relation. Also interesting are finite elasticity models in which

bending theory is used to investigate instability [**?** **?**].

However, all the aforementioned noteworthy theoretical models regarding large deformations have been formulated making reference to linear constitutive law or a plane strain condition or nearly incompressibility assumption. The 3D model for finite theory of bent solids [**?**] was extended to the case of slender solids in [**?** **?** **?**], and was also extended to slender viscous materials in [**?**].

Numerical discrete formulations and experimental test aimed to simulate and describe the effects induced by pure bending conditions are also noteworthy. A numerical solution of 3D bending and based of variational formulation was proposed in [**?** **?**] for a hyperelastic materials. Many experimental devices and standardised test have been proposed in the literature to subject a body to pure flexion without inducing axial or shear forces [**?** **?** **?** **?**].

The objectives of this work are: to improve the 3D model of finite bending of prismatic hyperelastic and compressible solids proposed recently in [**?**]; to provide the expression of the neutral loci in closed form; to highlight the nonlinear form of dimensionless moment vs *Eulerian slenderness* relation that is valid for any aspect ratio of the bent solid; to discuss limitations of the EE formulation through the new dimensionless bending moment vs Eulerian slenderness relation; to establish limits of use of the new theory of bending.

Conversely to [**?**], equilibrium conditions are made more robust by imposing vanishing of the axial force over the cross sections and discussing on the relevance of this new condition. Expressions of *neutral loci* which are not present in the literature in the context of finite elasticity, corresponding to unstretched and unstressed surfaces of the bent solid, are identified and provided in closed form as a function of the stored energy density function. Linearisation of the present model of a bent solid are provided leading to two approximated solutions: the EE and the NEE formulations. A new bending moment-curvature relation is provided accounting for transversal and longitudinal deformation of the solid. Once the constitutive parameters of the material are fixed, it is shown that the curve of dimensionless moment vs *Eulerian slenderness* is valid for any solid of any aspect ratio. In this curve, the present model exhibits a nonlinear trend.

Conversely, the Euler Elastica displays a linear trend. The present curve can be used in order to establish the limitations of the EE theory. Limit values in terms of Eulerian slenderness and compactness index are provided for the use of the present model.

The paper is organized as follows. In Section 2, analytic preliminaries concerning both the kinematics and statics of the theoretical formulation are presented. The kinematics of the problem has been described thoroughly in [**?**]. Nonetheless, assumptions and governing kinematic parameters are briefly recalled in Section 2.1. The reume of the kinematics and resumed in Appendix A for convenience. Appendix B describes the neutral loci of both kineamtics and mechanics of the present bending model of solids. The new mechanical model is presented in Section 2.2 by discussing the main differences with respect to [**?**] and supporting the importance of the new equilibrium conditions. The general bending moment-curvature relation is obtained in Section 3 and then specialised in Section 4 for a compressible Mooney-Rivlin (MR) material. Section 5 introduces the FE model whose results are compared with respect to present model and other formulations in Section 6. Finally, conclusion are drown in Section 7.

2. Analytic preliminaries

In the present Section kinematics and mechanics of uniformly bent hyperelastic solids are investigated. The kinematic model describes the assumptions of the bending model by which the deformation of the solid is considered. Thus, the unknowns of the model, its kinematic parameters, are introduced. The mechanical model is formulated for a homogeneous, isotropic and compressible hyperelastic material. Based on the deformation vector provided by the kinematics, the mechanical model provides a nonlinear system of equation representing equilibrium conditions of the solid. Therefore, the solution of the nonlinear system of equation provides the kinematic unknowns of the problem.

2.1. Kinematic model

A prismatic solid[1] of length L and rectangular cross section $B \times H$ is considered according to Figure 1. Reference is made to a Cartesian coordinate

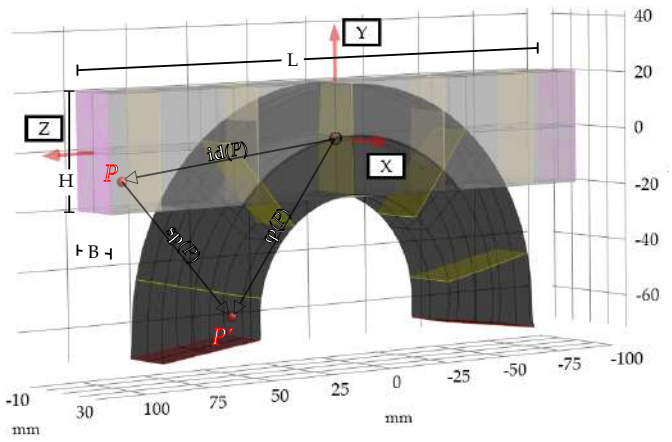

Figure 1: Prismatic solid subjected to finite bending: reference system $\{O, X, Y, Z\}$, reference configuration (grey solid) and deformed configuration (black solid).

system $\{O,\, X,\, Y,\, Z\}$ with the origin placed at the centroid of the solid. The solid is made of a hyperelastic, homogeneous and isotropic material. Each point $P \equiv (X,\, Y,\, Z)$, belonging to the reference configuration of the solid, is identified by the position vector $\mathbf{id}(P) = X\hat{\mathbf{i}} + Y\hat{\mathbf{j}} + Z\hat{\mathbf{k}}$, being $\hat{\mathbf{i}}$, $\hat{\mathbf{j}}$ and $\hat{\mathbf{k}}$ the unit vectors of the Cartesian axis. The displacement vector $\mathbf{sp}(P) = u(P)\,\hat{\mathbf{i}} + v(P)\,\hat{\mathbf{j}} + w(P)\hat{\mathbf{k}}$ (given in Table A.1) moves the point P to the deformed configuration $P' \equiv \big(x(P)\,, y(P),\, z(P)\big)$. The deformation vector $\boldsymbol{\varphi}(P) = x\hat{\mathbf{i}} + y\hat{\mathbf{j}} + z\hat{\mathbf{k}}$ identifies the point P' in the deformed configuration according to the map $\boldsymbol{\varphi}(P) = \mathbf{id}(P) + \mathbf{sp}(P)$, see Figure 1.

As depicted in Figure 2, due to the prescribed rotation α_0 of the final cross

[1]The term *solid* will be used in the following to remark the difference with respect to the term *beam* or *rod*, which are typically considered in framework of linearised elasticity or EE formulation. In particular, a beam or rod are a slender 3D elements whilst the solid is here assumed as non-slender 3D element without restrictions in terms of geometries.

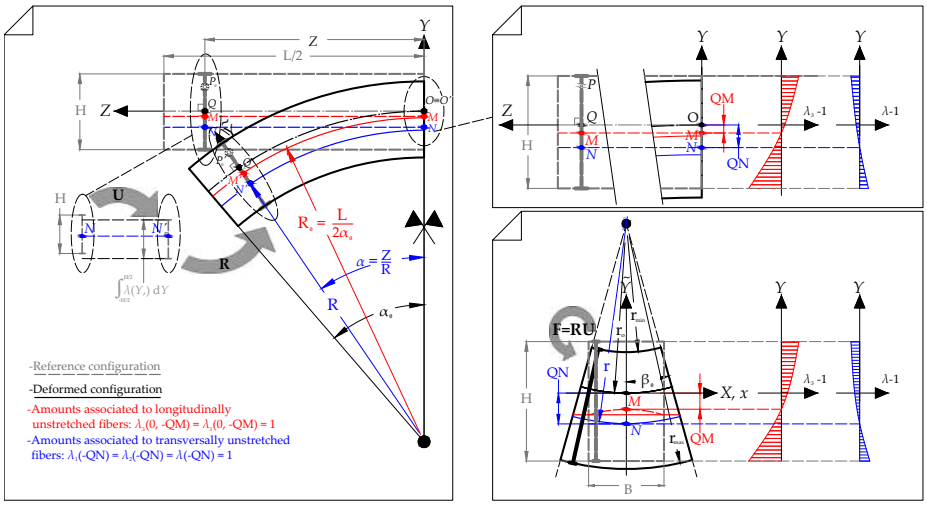

Figure 2: Kinematic model of a prismatic solid subjected to finite bending: (a) kinematics in the longitudinal ZY plane at $X = 0$; (b) detail about the unstretched fibres QN and QM and principal stretches distributions along the Y axis; (c) kinematics in the transverse $X\tilde{Y}$ planes.

sections of the body, the solid is bent in such way to deform by according to three main kinematic assumptions [**?**]: in the ZY planes the longitudinal radii of curvature are constants along the Z axis; cross sections of the solid remain plane after deformation; all the cross sections deform in the same way into sectors of a circular crown.

The displacement field is characterized by three kinematic unknowns that are determined by imposing equilibrium conditions. The Y coordinate of the unstretched fibre lying in the planes of the cross sections is denoted by QN and it is one of the unknowns of the problem. The transverse principal stretches, $\lambda_1(P)$ and $\lambda_2(P)$, turn out to be [**?**]

$$\lambda_1(Y) = \lambda_2(Y) = \lambda(Y) = \frac{r_O}{r} e^{-\frac{Y}{r}}, \tag{1}$$

being r_O the transverse radius of curvature associated to the centroid of the solid (see Table A.1) and r denotes the anticlastic radius of curvature associated to

the *transverse neutral fibre* $N \equiv (0,\, -QN,\, Z)$[2]. It follows that $\lambda(N) = 1$, see Figure 2. The anticlastic radius of curvature r is the second unknowns of the problem.

Along the Z direction, the fibre N is characterized by the longitudinal radius of curvature R that is the third unknown of the problem. An important role is played by the kinematic parameter QM (see eq.(B.1)) that denotes the Y coordinate corresponding to the longitudinal fibre lying in the YZ plane that preserves its length after deformation. Such a fibre is $M \equiv (0,\, -QM,\, Z)$ and it represents the *longitudinal neutral fibre* for which $\lambda_3(M) = 1$, being λ_3 the longitudinal principal stretch, which reads

$$\lambda_3(X, Y) = \frac{R + r}{R_0} - \frac{r_{\mathrm{O}}}{R_0} e^{-\frac{Y}{r}} \cos\beta, \tag{2}$$

being $\beta = X/r$. Final cross sections of the solid at $Z = \pm L/2$ and lateral surfaces of the solid at $X = \pm B/2$ rotate by the angles $2\,\alpha_0 = L/R_0$ and $2\beta_0 = B/r$, respectively, being R_0 the longitudinal radius of curvature associated to the fibre M, as depicted in Figure 2[3]. Therefore, the kinematic control parameters quantifying the flexure acting on the system is α_0 or, equivalently, R_0.

2.2. Mechanic model

The first Piola-Kirchhoff stress tensor $\mathbf{T}_R$ is given in terms of the constitutive law as

$$\mathbf{T}_R = \frac{\partial W}{\partial \mathbf{F}} = 2\left[(W_{,1} + I_1 W_{,2})\ \mathbf{F} - W_{,2}\mathbf{B}\,\mathbf{F}^{\mathrm{T}} + I_3 W_{,3}\,\mathbf{F}^{-\mathrm{T}}\right], \tag{3}$$

in which $\mathbf{F}$ is the deformation gradient, $\mathbf{B} = \mathbf{F}\mathbf{F}^T$ is the left Cauchy deformation tensor, and $W_{,i} = \partial W/\partial I_i$ denotes derivatives of the stored energy density function $W(I_1,\, I_2\, I_3)$ with respect to the deformation invariants I_i, with $i = 1, 2, 3$.

---

[2] For the details about the neutral fibres see Appendix B.

[3] It is remarked that both QM and QN are quantities defined in the reference configuration. In deformed configuration it follows $y(N) - y(M) = R_0 - R$. Conversely to the present formulation, in the beam model proposed in [**?** **?**] one has $QN = QM = 0$ and $R = R_0$.

The governing quantities of the mechanic model turn out to be the principal components of the Biot stress tensor, $\mathbf{T}_B = \mathbf{R}^{-1}\mathbf{T}_R$ [**?**], as reported in Table A.2. In particular, for the problem at hand, the Biot principal stresses assume the following form:

$$T_{B_1}(P) = 2\frac{r_O}{r^3}e^{-\frac{3Y}{r}}\left\{r^2 e^{\frac{2Y}{r}}\left\{W_{,1}+W_{,2}\left[\left(\frac{R+r-r_O e^{-\frac{Y}{r}}\cos\beta}{R_0}\right)^2+\left(\frac{r_O}{r}e^{-\frac{Y}{r}}\right)^2\right]\right\}+ W_{,3}\left(r_O\frac{R+r-r_O e^{-\frac{Y}{r}}\cos\beta}{R_0}\right)^2\right\}, \quad (4)$$

$$T_{B_3}(P) = \frac{2e^{-\frac{5Y}{r}}\left[(r+R)e^{\frac{Y}{r}}-r_O\cos\beta\right]}{r^4 R_0}\left[\left(re^{\frac{Y}{r}}\right)^4 W_{,1}+2\left(r\,r_O e^{\frac{Y}{r}}\right)^2 W_{,2}+r_O^4 W_{,3}\right]. \quad (5)$$

Note that T_{B_2} corresponds with T_{B_1} as a consequence of the main assumptions of the model. Similarly to the principal stretches (1) and (2), also the principal stresses (4) and (5) are even functions of the X coordinate. Both principal stretches and stresses do not depend on the Z coordinate because of the uniform bending.

As thoroughly investigated in [**?**], a nonlinear system of three equations is achieved by imposing the equilibrium conditions. The solution of this nonlinear system provides the kinematic unknowns R, r, and QN.

The first equation of the nonlinear system involves the material divergence of the stress tensor $\mathbf{T}_R$. Making reference to the transverse neutral fibre N, under the assumption of zero body forces, it was shown in [**?**] that the indefinite equilibrium equations reduce to

$$\frac{T_{B_1}}{r} = \frac{T_{B_3}}{R_0}, \qquad \text{for } N \equiv (0,\, -QN,\, Z), \quad (6)$$

which, in terms of the stored energy function, turns out to be

$$W_{,1}+W_{,2}\frac{2R_0^2}{r\,R}+W_{,3}\left(\frac{2R}{r}-1\right)+W_{,11}\left(\frac{4R_0^2}{rR}-2\right)+2\,W_{,12}\left(\frac{4R_0^2+2R^2}{R\,r}- \frac{R^2}{R_0^2}-2\right)+W_{,13}\left(\frac{8R}{r}-\frac{2R^2}{R_0^2}-2\right)-W_{,22}\frac{2\left(R^2+R_0^2\right)\left(rR-2R_0^2\right)}{rRR_0^2}+ 2W_{,23}\left[\frac{2R\left(2R_0^2-rR+R^2\right)}{rR_0^2}-1\right]-W_{,33}\frac{2R^2(r-2R)}{rR_0^2}=0. \quad (7)$$

The equilibrium equations at the free surfaces of the solid are fulfilled by imposing vanishing circuitry of the Piola-Kirchhoff stress vector $\mathbf{t}_R = \mathbf{T}_R\mathbf{n}$, being $\mathbf{n}$ the unit normal at the boundaries of the body. By imposing such a condition one has

$$\oint_{\mathcal{L}} \mathbf{t}_R \, d\mathcal{L} = \int_{-H/2}^{+H/2} T_{B_1}(B/2, Y) \, dY - \big[o(QN/r) + o(H/r)\big] = 0. \tag{8}$$

Conversely to [**?**], the last equation required for the solution of the problem is the vanishing of the axial force N over the cross sections[4], namely

$$N = \int_A T_{B_3}(X\,, Y) \, dA = 0. \tag{9}$$

It will be shown that condition (9), that was not considered in [**?**], significantly increases the accuracy of theoretical model for prediction of stretches and stresses also for very short solids under extremely large deformations. Thereby, the problem of flexure of solids is handled by solving numerically the coupled system of nonlinear eqns.(7), (8), and (9) in the kinematic unknowns R, r, and QN.

Let us discuss about the nonlinear distribution of the stress component $T_{B_3}(0,\, Y)$ along the Y axis in order to show the relevance of eq.(9). The nonlinearity of the stress distribution within the height of the solid increases as the rotation angle α_0 increases, as sketched qualitatively in Figure 3(a). Such a figure highlights the *partialization* of the cross section: upper portion of the solid is subjected to tension whereas lower portion is prone to compression.

As known, the most part of materials under moderate deformations are characterised by a uniaxial stress-stretch curve ($T_{R_{33}}\, vs\, \lambda_3$) that exhibits softening

[4] In the initial version [**?**] of the present model , eq.(9) was not considered. A geometrical consideration about the *almost linearity* of the transversal principal stretch distribution was assumed leading to the following condition:

$$\frac{1}{2}\left[e^{-\frac{1}{r}\left(QN+\frac{H}{2}\right)} + e^{-\frac{1}{r}\left(QN-\frac{H}{2}\right)}\right] \cong 1.$$

Such an assumption leads to accurate predictions only for moderate deformations and solids with compact cross sections.

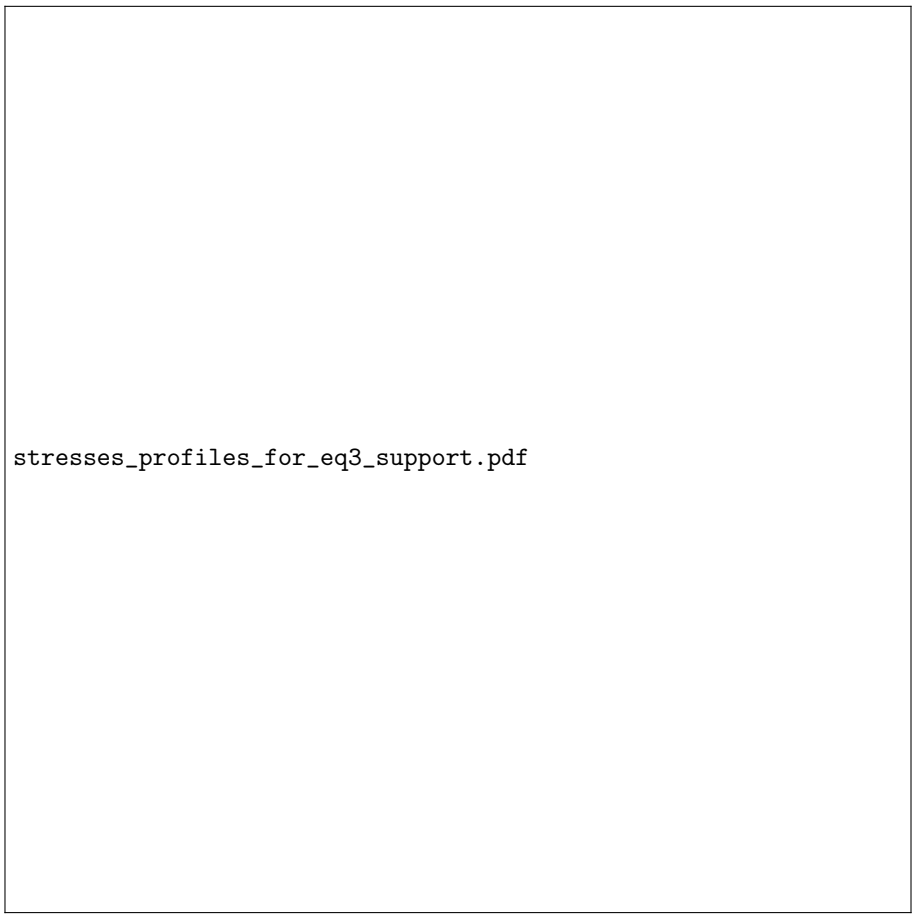

Figure 3: Distribution of the longitudinal stress $T_{B_3}(X, Y)$: (a) evolution of the stress distribution at $X = 0$ and motion of the unstressed point QM_R as the prescribed rotation α_0 increases; (b) stress distribution at $X = 0$ in case of balance between compressive and tensile longitudinal stress resultants (solid line), nonlinear unbalanced stress distribution (dotted line), and linear balanced stress distribution (dashed line).

under tension and hardening under compression. It follows that the balance of normal tractions over the cross section can be fulfilled only if the unstressed fibre (QM_R in Figure 3) moves toward the bottom of the cross section as the deformation increases[5]. This is the only way to ensure the balance between the

[5]The considerations regarding the stress distribution across the height of the cross section

resultant of normal traction inside the compressed region ($\mathrm{N_c}$ in Figure 3(b)) and resultant of normal traction of region under tension ($\mathrm{N_t}$). If the unstressed fibre is assumed *a priori* at $Y = 0$, the nonlinear (and monotonic) stress distribution turns out to be unbalanced, as sketched by the dotted curve in Figure 3(b)[6].

The balance of the normal tractions should be investigated not only at the coordinate $X = 0$ but over the entire cross section of the solid. However, due to a week dependence of the longitudinal stress from the X coordinates[7], the normal tractions over a vertical segment directed along Y do not vary relevantly. This variation takes relevance as the width of the solid increases with respect to the height, namely namely for great values of the compactness index $\beta_{\mathrm{C}} = B/H$. For solids with large values of β_{C}, the coordinates QM_R can also be placed at $Y > 0$ (see Figure B.13).

Relation $\mathbf{id}(P) = \boldsymbol{\varphi}(P) - \mathbf{sp}(P)$ provides Eulerian coordinates x, y, and z as a function of Lagrangian coordinates X, Y and Z (see Table A.1). Moreover, based on the first Piola-Kirchhoff stress tensor $\mathbf{T}_R$ (3), the Cauchy stress tensor $\mathbf{T}(P')$ follows from the well known relation $\mathbf{T} = \mathbf{T}_R\,\mathbf{F}^{\mathrm{T}}/\det(\mathbf{F})$. In particular, in the principal reference system, Cauchy stress tensor assumes the following diagonal form:

$$[\mathbf{T}] = \begin{bmatrix} T_1 & 0 & 0 \\ 0 & T_1 & 0 \\ 0 & 0 & T_3 \end{bmatrix} = \begin{bmatrix} \dfrac{T_{B_1}}{\lambda\lambda_3} & 0 & 0 \\ 0 & \dfrac{T_{B_1}}{\lambda\lambda_3} & 0 \\ 0 & 0 & \dfrac{T_{B_3}}{\lambda^2} \end{bmatrix}, \tag{10}$$

(see also Section 4.3) are relevant in order to explain the unbalanced stress profile provided by the nonlinear Euler *Elastica* formulation.

[6] It is remarked that a compressive behaviour in hardening and tensile behaviour in softening with monotonic trend has been assumed.

[7] It is observed that the dependence on the X coordiante of the stress distribution is intruded by the principal stretches (1) and (2) through the term $\cos(X/r)$. Therefore, due to the smallness of the term X/r, a week dependence on X characterises the stress distribution inside the cross section.

or equivalently in terms of Cauchy principal stress components

$$T_i \;\; = \frac{T_{B_i}}{\lambda_i}\left(\frac{\delta_{i1}}{\lambda_3}+\frac{\delta_{i3}}{\lambda_i}\right) \text{ (no summation)},$$

being δ_{ij} the Kronecker symbol ($i = 1$ and 3)[8]. In (10), the principal stretches λ_i are given in terms of Eulerian coordinates as

$$\lambda(P') \;\; = \;\; \sqrt{\frac{x^2+\left[R+r-\sqrt{z^2+(y+R+r-r_{\mathrm{O}})^2}\right]^2}{r^2}}, \tag{11}$$

$$\lambda_3(P') \;\; = \;\; \sqrt{\frac{z^2+(y+R+r-r_{\mathrm{O}})^2}{R_0^2}}. \tag{12}$$

In the next Section, based on the above expressions, bending moment-curvature relation will be obtained.

3. Bending moment-curvature relation of a bent solids

The kinematic and mechanic models of the previous section are used in the current section for the definition of the bending moment-curvature relation of a uniformly bent hyperelastic solid.

The bending moment is evaluated making reference to the deformed configuration of the cross section. Therefore, considering the Cauchy stress component T_3 given in eq.(10), the moment-curvature relation reads[9]

$$m_x(R_0) = \int_{A'} \hat{y}(P')\, T_3(P')\, dA', \tag{13}$$

being $\hat{y} = \tilde{y}_P - \tilde{y}_M$ the arm of the Cauchy stress T_3 with respect to the longitudinally unstretched fibre and A' the deformed cross section area. Making

[8] At $Z = 0$ principal directions of Cauchy stress tensor correspond to the Cartesian axes XYZ. Observing the stress component T_3 in eq.(10), it follows that Biot stress component T_{B_3} governs the position of the unstressed fibre in both reference and deformed configuration (as discussed in Appendix B).

[9] It is recalled that the problem at hand accounts for uniform bending, thus the bending moment does not depend on the Z coordinate ($Z = z = 0$ can be assumed to handle formula (13)).

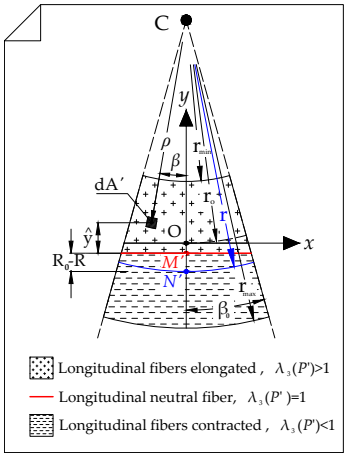

Figure 4: Deformed configuration of a generic cross section: polar reference system $\{C,\, \rho,\, \beta\}$ for the evaluation of the bending moment with longitudinally fibres elongated and contracted.

reference to the polar reference system $\{C,\, \rho, \beta\}$ of Figure 4, Eulerian principal stretches (11) and (12), Cauchy stress component T_3, and its arm turn out to be

$$\lambda(\rho,\beta) = \sqrt{\frac{(\rho\sin\beta)^2+(\rho\cos\beta-r+r_{\rm O})^2}{r^2}}, \quad \lambda_3(\rho,\beta)=\frac{R+2r-r_{\rm O}-\rho\cos\beta}{R_0},$$

$$T_3(\rho,\,\beta) = \frac{2(\rho\cos\beta-2r-R+r_{\rm O})}{r^2R_0\left[\rho^2\sin^2\beta+(\rho\cos\beta-3r-2R+r_{\rm O})^2\right]}\Big\{r^4W_{,1}+2r^2\Big[\rho^2\sin^2\beta+$$
$$(\rho\cos\beta-r+r_{\rm O})^2\Big]W_{,2}+\Big[\rho^2\sin^2\beta+(\rho\cos\beta-r+r_{\rm O})^2\Big]^2W_{,3}\Big\}, \quad (14)$$

$$\hat{y}(\rho,\,\beta) = r-\rho\cos\beta-(R_0-R). \quad (15)$$

Thus, the introduction of relations (14) and (15) into (13) provides the most general form of the nonlinear moment-curvature relation as

$$m_x(R_0) = 4\int_0^{\beta_0}\int_{r_{\rm min}}^{r_{\rm max}} \frac{\rho\,(r+R-R_0-\rho\cos\beta)\,(\rho\cos\beta-2r-R+r_{\rm O})}{r^2R_0\left[\rho^2\sin^2\beta+(\rho\cos\beta-3r-2R+r_{\rm O})^2\right]}\times$$
$$\Big\{r^4W_{,1}+2r^2\Big[\rho^2\sin^2\beta+(\rho\cos\beta-r+r_{\rm O})^2\Big]W_{,2}+$$
$$\Big[\rho^2\sin^2\beta+(\rho\cos\beta-r+r_{\rm O})^2\Big]^2W_{,3}\Big\}\,d\rho\,d\beta, \quad (16)$$

being $r_{\rm min}$ and $r_{\rm max}$ the minimum and maximum anticlastic radii of curvature of the fibres at $Y=\pm H/2$ respectively (see Table A.1).

Conversely to the *Elastica*, the moment-curvature relation (16) is coupled with the kinematic unknowns QN, r, and R provided by the solution of the nonlinear system of eqns. (7), (8) and (9).

4. Application to a compressible Mooney-Rivlin material

In the present section the stored energy density function $W(I_1, I_2, I_3)$ is specialised to the case of compressible Mooney-Rivlin (MR) material. Firstly, the form of the MR energy is achieved starting from its original definition and adding the contribution of the compressibility. Secondly, the mechanical model and, in turn, moment-curvature relation are specialised to the case of MR material. Finally, approximations of present theory of bending will be introduced leading to the nonlinear Euler Elastica and Euler Elastica theories.

4.1. Stored energy function

Let us consider a compressible Mooney-Rivlin (MR) material characterized by the stored energy density function [**?**]

$$W(I_1, I_2, I_3) = aI_1 + bI_2 + \Gamma(I_3) + \omega_0, \quad a > 0, b > 0, \omega_0 \in \mathbb{R}, \tag{17}$$

in which $\Gamma :]0, +\infty[\to \mathbb{R}$ is a polyconvex function satisfying $\Gamma(I_3) \xrightarrow{I_3 \to 0^+} +\infty$ that introduces the dependence on the third invariant of deformation as [**?**]

$$\Gamma(I_3) = cI_3 - \frac{d}{2}\log(I_3), \quad c > 0, d > 0. \tag{18}$$

Constants d and ω_0 in (17) and (18) follow from the conditions of vanishing energy and absence of traction when $\lambda = \lambda_3 = 1$, as shown in [**?**]. These conditions lead to

$$\begin{cases} \omega_0 = -3(a+b) - c \\ d = 2(a + 2b + c) \end{cases},$$

from which the final form of the MR stored energy density reads

$$W(I_1, I_2, I_3) = a(I_1 - 3) + b(I_2 - 3) + c(I_3 - 1) - (a + 2b + c)\log(I_3). \tag{19}$$

From (19), the derivatives of W required for the computation of the stress component and bending moment given in the previous Sections assume the following form:

$$
\begin{aligned}
&W_{,1} = a, \quad W_{,2} = b, \quad W_{,3} = c - \frac{r^4\, R_0^2\, e^{\frac{6Y}{r}}\,(a+2b+c)}{r_{\rm O}^4\left[(r+R)\,e^{\frac{Y}{r}} - r_{\rm O}\cos\beta\right]^2},\\
&W_{,11} = W_{,13} = W_{,12} = W_{,22} = W_{,23} = 0,\\
&W_{,33} = \frac{r^8\, R_0^4\, e^{\frac{8Y}{r}}\,(a+2b+c)}{r_{\rm O}^8\left(r+R-r_{\rm O}\,e^{-\frac{Y}{r}}\cos\beta\right)^4},
\end{aligned}
\tag{20}
$$

4.2. Mechanics of the bending model of solids

The derivatives (20) of the stored energy allow to obtain the principal components of the Biot stress tensor (4) and (5) for a MR material as

$$
\begin{aligned}
T_{B_1}(X,\,Y) \;=\;& \frac{2\,r}{r_{\rm O}}e^{\frac{Y}{r}}\left\{a\left(\frac{r_{\rm O}^2 e^{-\frac{2Y}{r}}}{r^2}-1\right)+b\left(\frac{r_{\rm O}^4 e^{-\frac{4Y}{r}}}{r^4}-2\right)-c+\right.\\
&\left.\frac{r_{\rm O}^2 e^{-\frac{6Y}{r}}\left(b\,r^2 e^{\frac{2Y}{r}}+c\,r_{\rm O}^2\right)\left[(r+R)e^{\frac{Y}{r}}-r_{\rm O}\cos\beta\right]^2}{r^4 R_0^2}\right\},
\end{aligned}
\tag{21}
$$

$$
\begin{aligned}
T_{B_3}(X,\,Y) \;=\;& \frac{2R_0(a+2b+c)}{e^{-\frac{Y}{r}}\,r_{\rm O}\,\cos\beta - r - R} + \frac{2}{R_0}\left[R+r-r_{\rm O}\,e^{-\frac{Y}{r}}\,\cos\beta\right]\times\\
&\left[a+\frac{r_{\rm O}^2 e^{-\frac{4Y}{r}}\left(2b\,r^2 e^{\frac{2Y}{r}}+c\,r_{\rm O}^2\right)}{r^4}\right].
\end{aligned}
\tag{22}
$$

The nonlinear system of three equations for the solution of the problem can be achieved by introducing (21) and (22) into eqns.(6) and (8), namely

$$
\begin{cases}
R_0^2(2a+5b+c)+R\,[R(b+3c)-2r(b+c)]=0\\
R_0-R=r\,(1-\cos\beta_0)\\
\displaystyle\int_A T_{B_3}(X\,,Y)\,dA=0
\end{cases}
\quad .
\tag{23}
$$

Finally, numerical solution of system (23) provides the kinematic unknowns QN, r, and R.

Let us remark some aspects about system (23). Based on the ratio between the longitudinal and transversal radii of curvature [**?**], eq.$(23)_1$ can be inter-

preted as the *nonlinear Poisson ratio* for a MR material, namely

$$\nu_{\mathrm{MR}} = \frac{2c + 2(a+3b+c)\frac{R_0^2}{R^2}}{(c-a) + (a+2b+c)\frac{R_0^2}{R^2}}, \tag{24}$$

that varies with the deformation. Moreover, eq.(8) admits the following two solutions:

$$r\,(1-\cos\beta_0) + R = \pm R_0. \tag{25}$$

However, the left hand side of eq.(25) is always positive. Therefore, the only admissible solution of (8) is eq.$(23)_2$. As a consequence, the following inequality holds true:

$$R_0 > R. \tag{26}$$

Relation (26) means that longitudinal neutral fibre M' lies above the transversal neutral fibre N', as sketched in Figure 2. Finally, despite its unmanageable form, expression $(23)_3$ can be easily computed using a symbolical manipulator.

The moment-curvature relation is then obtained by substituting into (16) relation (20), thus providing

$$\begin{aligned} m_x(R_0) \;=\; & \frac{4}{r^2 R_0}\int_0^{\beta_0}\int_{r_{\mathrm{Min}}}^{r_{\mathrm{Max}}} \frac{\rho\,(r+R-R_0-\rho\cos\beta)\,(\rho\cos\beta-2r-R+r_{\mathrm{O}})}{\rho^2\sin^2\beta+(\rho\cos\beta-3r-2R+r_{\mathrm{O}})^2}\times \\ & \left\{ a\,r^4 + \left[\rho^2\sin^2\beta+(\rho\cos\beta-r+r_{\mathrm{O}})^2\right]\left\{ 2\,b\,r^2+\left[\rho^2\sin^2\beta+(\rho\cos\beta-r+r_{\mathrm{O}})^2\right]\times \right.\right. \\ & \left.\left. \left[c - \frac{r^4 R_0^2(a+2b+c)}{\left[\rho^2+2\rho\cos\beta(r_{\mathrm{O}}-r)+(r-r_{\mathrm{O}})^2\right]^2\,(\rho\cos\beta-2r-R+r_{\mathrm{O}})^2}\right]\right\}\right\} d\rho\,d\beta. \end{aligned} \tag{27}$$

4.3. Approximations of the bending theory of solids

The linearisation of the present model allows us to introduce two different approximations of the modelling of bending: the *nonlinear Euler Elastica* (NEE) and the well known *Euler Elastica* (EE). Both the approximated formulations are achieved by imposing in the present model the condition $QN = 0$ which, in turn, implies $R_0 = R$ and $QM = 0$. In addition, linearisation of stretches and displacements is performed with respect to the dimensionless variables X/r and

Y/r by expanding them in Taylor series and truncating the obtained expressions up to $o(X/r)^2$ and $o(Y/r)^2$.

The difference between EE and NEE formulation stands in the constitutive law. Starting from the present formulation, the EE theory is retrieved by linearising the principal stretches (1) and (2), thus obtaining the principal stress T_{B_3} based on a linear constitutive law. This corresponds to the linearisation of T_{B_3}, namely by truncating series expansion of eq.(22) up to $o(X/r)^2$ and $o(Y/r)^2$. Conversely, the NEE formulation is obtained with the same aforementioned linearisation of the stretches but assuming the nonlinear stress component T_{B_3} consistently with respect the constitutive law (3).

The investigation of the equilibrium conditions (23) for the linearised cases of EE and NEE allows to explain the limitation of the approximated theories. For both EE and NEE formulations, the assumption of $R_0 = R$ transforms eq.$(23)_1$ into the following relation:

$$r = \frac{a + 3b + 2c}{b + c} R. \tag{28}$$

Thus, relation (28) reduces the kinematic unknowns to the sole radius of curvature R, which becomes the control kinematic parameter of the problem. Similarly to (24), eq.(28) defines the *linearised Poisson ratio* for a compressible MR material as

$$\nu_{\mathrm{MR}} = \frac{b + c}{a + 3b + 2c}. \tag{29}$$

Moreover, as shown in [**?** **?**] and in the following, the linearization of the constitutive law leads to the *linearised Young modulus* of a MR material

$$E_{\mathrm{MR}} = \frac{4(a + b)(a + 4b + 3c)}{a + 3b + 2c}. \tag{30}$$

Combination of eqns.(29) and (30) gives the *linearised Lamé constants* of a compressible MR material as[10]

$$\mu_{\mathrm{MR}} = 2(a + b), \quad \lambda_{\mathrm{MR}} = 4(b + c). \tag{31}$$

[10]Note that the *linearised Shear modulus* $(31)_1$ is consistent with the well known formula $\mu = 2(W_{,1} + W_{,2})$ [**?**].

Due to assumption $R_0 = R$, eq.$(23)_2$ is fulfilled. For both the EE and NEE theories, eq.$(23)_3$ will be discussed in the following based on the approximated forms of the stress component T_{B_3} of (22).

4.3.1. Nonlinear Euler Elastica (NEE)

By expanding in power series the principal stretches (1) and (2) one has

$$\lambda = 1 - \frac{Y}{R}\nu_{\mathrm{MR}}, \qquad \lambda_3 = 1 + \frac{Y}{R}. \tag{32}$$

Accordingly with 32, evaluating the deformation invariants I_i, the deformation gradient $\mathbf{F}$, and the right Cauchy deformation tensor $\mathbf{B}$ provides the expression of the stress component T_{B_3} as

$$T_{B_3} = 2\left(\frac{Y}{R}+1\right)\left\{a + \left(1-\frac{Y}{R}\nu_{\mathrm{MR}}\right)^2\left[2b + c\left(1-\frac{Y}{R}\nu_{\mathrm{MR}}\right)^2\right]\right\} + \frac{\lambda_{\mathrm{MR}} R\,(\nu_{\mathrm{MR}}-1)}{2\nu_{\mathrm{MR}}(R+Y)}. \tag{33}$$

The stress component (33) allows to compute the nonlinear bending moment according to the NEE theory as

$$\begin{aligned} m_{\mathrm{NEE}}(R) \;=\; & B\left\{\frac{H^5\nu_{\mathrm{MR}}^2}{20R^3}\left[b + c(3-2\nu_{\mathrm{MR}})\right] + \frac{cH^7\nu_{\mathrm{MR}}^4}{224R^5} - \frac{\lambda_{\mathrm{MR}}}{2\nu_{\mathrm{MR}}}\left[\frac{H^3}{3R}\left(\frac{\nu_{\mathrm{MR}}-1}{4} + \right.\right.\right. \\ & \left.\left.\left.\nu_{\mathrm{MR}}^2\right) + (\nu_{\mathrm{MR}}-1)R^2\log\left(\frac{2R-H}{H+2R}\right) + H(\nu_{\mathrm{MR}}-1)R\right]\right\}. \end{aligned} \tag{34}$$

4.3.2. Euler Elastica (EE)

The *Euler Elastica* is achieved starting from the linearised principal stretches (32) and then introducing the linear constitutive law[11] for an isotropic material. The resulting longitudinal stress component T_{B_3} corresponds to the linearisation of the stress component (22), namely

$$T_{B_3} = \frac{Y}{R}\mathrm{E}_{\mathrm{MR}}, \tag{35}$$

where E_{MR} is given by relation (30). Eq.(35) complies with the Bernoulli-Navier linearised stress-strain relation. Accordingly, the moment-curvature relation

[11] The linearisation of the constitutive law leads to a number of analytical paradoxes [**?** **?**] as the violation of principle of material indifference.

(13) provided by the EE formulation gives the well known formula

$$m_{\mathrm{EE}}(R) = \frac{\mathrm{E_{MR}} J_X}{R}, \tag{36}$$

being J_X the moment of inertia of the rectangular cross section. The results provided by the above formulations will be compared in Section 6 with respect to results of finite element simulations.

5. Finite element model

The finite element model used as a comparison term with respect to the theoretical formulations of the previous Section is introduce in the current section.

The numerical simulations have been carried out with the finite element code COMSOL Multiphysics® v.5.6. Because of symmetry conditions, only one fourth of the solid have been modelled, see Figure 5. A user defined material

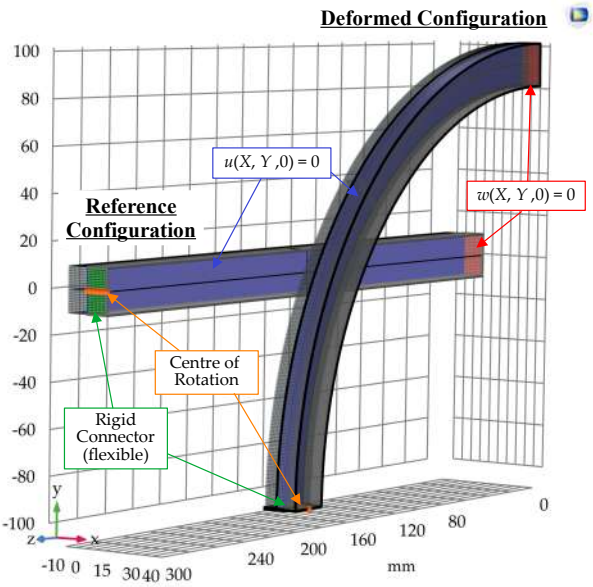

Figure 5: Reference and deformed configurations of the FE model: restraints, rigid connector and its centre of rotation.

has been associated to the solid. Such a material allows the implementation

of the stored energy density (19) as a function of the principal stretches of the solid.

Meshes are created using hexagonal brick elements characterized by a quality ratio of 0.99. The meshes are realized by dividing the minimum side of the block into 20 elements. Cubic serendipity shape functions have been used.

In terms of restraints, displacement components normal to each plane of symmetry are neglected, see blue and red surfaces of Figure 5. The bending is imparted by using flexible rigid connectors. The flexible rigid connector is applied to the final cross section of the solid and it allows in-plane deformations, see green surfaces of Figure 5. This feature is associated to a moving centre of rotation that lies on an axis parallel to X direction. In addition, Y component of the displacement of the centre of rotation is neglected. The rotation α_0 is thus applied to the cross section by the rigid connector. Thus, a static incremental analysis is performed by increasing the values of the prescribed rotation.

The Eulerian bending moment provided by the FE model is obtained by the following strategy: the deformed cross section at $Z = 0$ is partitioned in a number of elements of area A'_i; Cauchy stress tensor component T_{3i} at the centroid of each element A'_i is assessed; distances $\hat{y}_i$ of each centroid of elements A_i from the neutral line for which $\lambda_3(x, y, 0) = 1$ are extracted; finally, the bending moment is assessed as

$$m_{\mathrm{FE}}(R_0) = \sum_{k=1}^{K} \hat{y}_k \, T_{3k} \, A'_k, \tag{37}$$

being K the number of surface elements used for the discretization of the deformed cross section.

6. Results and discussion

Comparisons between results obtained with theoretical models and FE simulations are provided in the present Section in terms of non-vanishing axial force, distribution of stretches and stress, and bending moment-curvature relation.

For sake of definiteness, the constitutive parameters of a MR material in agreement with [**?**] are $a = 456.9$, $b = 381.1$ and $c = 317.6$ kPa. The geometries of the solid are chosen by fixing $B = 20$ mm and the ratio $L = 600$ mm. Only the height of the solid will be changed, thus introducing different investigated cases.

Three different cases are considered, as shown in Figure 6. Case (I) is char-

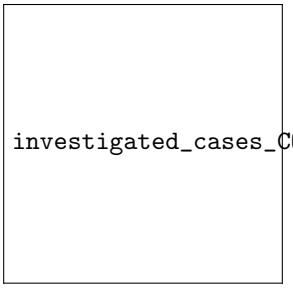

Figure 6: Reference and deformed configurations of the FE models for the investigated cases for $\alpha_0 = 180^{\circ}$: (a) case (I): $H = B/4$; Case (II): $= B$; Case (III): $H = 4B$. For each cases $B = 20$ mm and $L = 600$ mm. Contour plot are referred to the norm of the displacement vector.

acterized by a compactness index [**?**] $\beta_{\mathrm{C}} = B/H = 4$ and it resembles a slender slab slender solid. Case (II) is has a compactness index $\beta_{\mathrm{C}} = 1$ and it denotes a slender beam with compact cross section. Case (III) is characterized by $\beta_{\mathrm{C}} = 1/4$ and it represents a squat solid similar to a wall beam element.

Comparison is performed among results provided by FE simulations and three theoretical models: present theory of bendinf of solids (S); nonlinear Euler *Elastica* (NEE) formulation of Section 4.3.1; Euler *Elastica* (EE) formulation of Section 4.3.2. Although the FE solution is not an exact solution, it is assumed as reference solution. Thus, given a compared field f, the relative error associated to each theoretical model will be defined as $\varepsilon_{r,\,f} = 1 - f_{\mathrm{Th}}/f_{\mathrm{FEM}}$, being f_{Th} and f_{FEM} the value assumed by the field in case of FE and theoretical solution respectively.

Figure 7 shows the axial force N (defined in eq. (9)) normalized with respect to $E_{\mathrm{MR}}A$. In such a way, the normalization of the axial force makes the

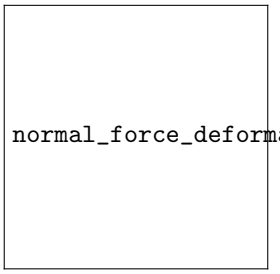

Figure 7: Normalised axial force (N) as a function of the curvature $\chi_0 = 1/R_0$ in case of bending model for solids (S), nonlinear Euler *Elastica* (NEE), and finite element (FE): (a) case (I) with $H = B/4$; case (II) with $H = B$; case (III) with $H = 4B$. For each cases $B = 20$ mm and $L = 600$ mm.

dimensionless quantity $N/E_{\mathrm{MR}}A$ similar to the definition (in the framework of linearised elasticity) of axial deformation induced by an axial force N. The results provided by the *Elastica* are omitted in Figure 7 since it provides a linear distribution of normal stresses which, in turn, gives a vanishing axial force.

Present model S and FE simulations provide vanishing or negligible normalised axial forces as depicted in Figs.7. This is ensured by equilibrium condition (9) for the model S and by the regime of pure bending simulated by the FE models. If the resultant of longitudinal stress assumes relevant values the investigated case would not represent a pure bending regime.

The NEE formulation, red curves in Figure 7, provides a residual axial force which grows as the curvature increases. This clearly does not agree with the pure pure bending regime. For a fixed value of the curvature $\chi_0 = 1/R_0$, the errors of NEE formulation increase from case (I) (Figure 7(a)) to case (III) (Figure 7(c)) due to decreasing *Eulerian slenderness* $\beta_{\mathrm{ES}} = R_0/H$ [**?**]. Indeed, by introducing relation (33) into (9), the normalised axial force provided by the NEE theory turns out to be

$$\frac{N}{\mathrm{E_{MR}A}} = -\beta_{\mathrm{ES}}^{-2}\left\{\frac{1}{1-2\nu_{\mathrm{MR}}^2-\nu_{\mathrm{MR}}}\left[\frac{1}{24}+\nu_{\mathrm{MR}}^2\left(\frac{1}{8}-\frac{\nu_{\mathrm{MR}}}{3}\right)\right]-\frac{2\,b\,\nu_{\mathrm{MR}}^2}{3\,\mathrm{E_{MR}}}\right\}. \quad (38)$$

Eq.(38) clearly shows that the normalised axial force, closer to an axial strain measure, increases as the Eulerian slenderness decreases. Recalling the bounds of the linearised Poisson ratio, $0 \leq \nu_{\mathrm{MR}} \leq 0.5$, it follows that eq.(38) turns

out to be always negative. This circumstance reveals an excess of compressive axial force. This unbalanced state of stress is generated by the approximations lying in the NEE formulation due to the impossibility to fulfil vanishing of the resultant of the longitudinal stress, i.e. eq.(9).

Figure 8 shows the longitudinal principal stretch $\lambda_3(0, Y)$ for five values of prescribed rotation α_0 of the final cross sections of the solid. Excepted for case

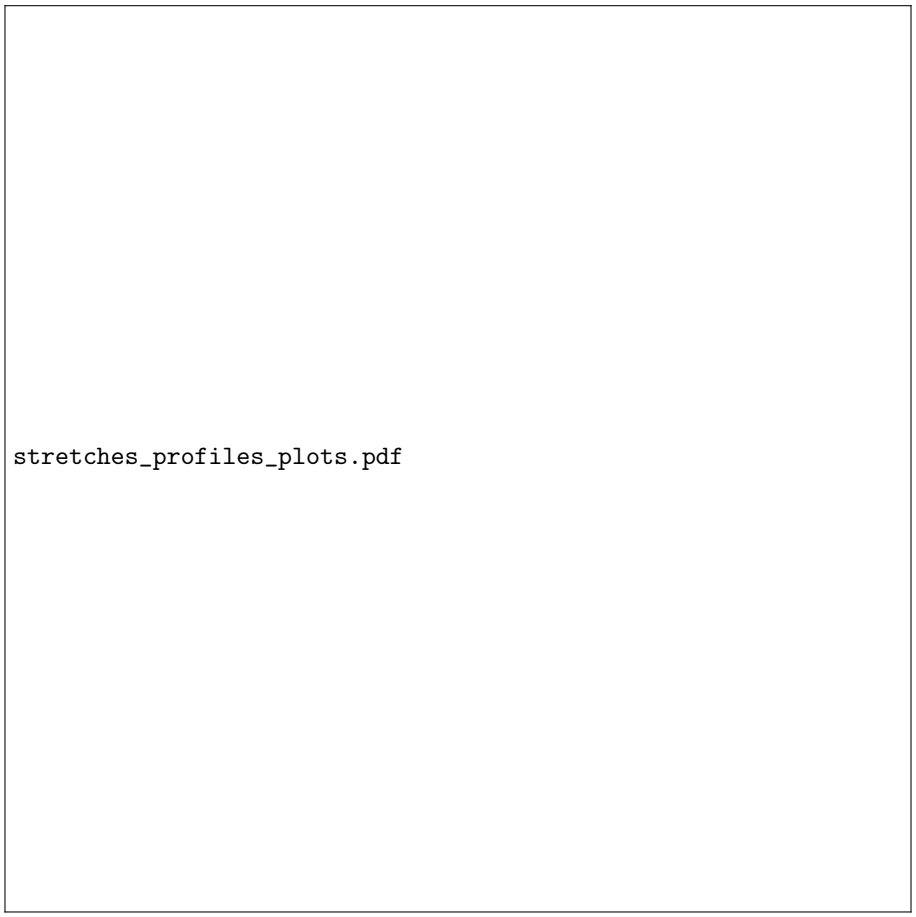

Figure 8: Comparison in terms of longitudinal principal stretch $\lambda_3(0, Y)$ for $\alpha_0 = \{15^o, 45^o, 90^o, 120^o, 180^o\}$ in case of bending model for solid (S), the Euler *Elastica* (EE), nonlinear Euler Elastica (NEE), and finite element (FE): (a) case (I) with $H = B/4$; case (II) with $H = B$; case (III) with $H = 4B$. For each cases $B = 20$ mm and $L = 600$ mm.

(III) reported in Figure 8(c), for low values of α_0 all formulations predict the

same distribution of the principal stretch λ_3 through-the-thickness of the solid that are almost linear. It is remarked that only the stretch profiles provided by the EE solution are exactly linear.

Despite of the similarity in terms of stretch distributions shown in Figs. 8(a) and 8(b), relevant differences arise among cases (I) and (II). The coordinate $Y = -QM$ of eq.(B.1), i.e. the position of the unstretched longitudinal fibre, increase its value as the deformation increases moving toward the negative Y, as clearly shown in Figure B.13(a). While for cases (I) and (II) the value of QM can be considered negligible, in the case (III) QM reaches values close to $0.08\,H$ when $\alpha_0 = 180^o$. Thereby, in case of non-slender solid the kinematic must be capable to grasp the motion of the unstretched fibre.

The stress distributions of the investigated cases are reported in Figure 9. For case (I), as for the stretches distribution of Figure 8(a), also the stress profiles of Figure 9(a) maintain a quasi-linear behaviour for each proposed solution. The capability to accurately predict the stress of the EE and NEE models slightly gets worse for case (II) of Figure 9(b). For the investigated prescribed angles, EE and NEE are able to predict the distributions of stretches and stresses for case (I) and (II).

For case (III), significant errors affect both the EE and NEE formulations, as shown in Figure 9(c). In particular these errors increase as the prescribed rotation increases. This is ascribed to the incapability of such formulations to grasp properly the coupling between kinematics and constitutive law that provides stresses. By carefully observing Figs.3, 7(c), 8(c), and 9(c) limitations of EE and NEE are evident. EE dramatically fails in the description of the stress distribution owing to the approximations affecting both kinematics and constitutive behaviour of the material. Conversely, when deformation becomes large, the fail of NEE shows that without a proper kinematics, the nonlinear constitutive law is not sufficient to increase the accuracy of the theoretical prediction.

The unreliability of the EE and NEE formulation to grasp stresses and stresses could also be observed for slender solids when high values of curvature are reached. The reliability of EE and NEE does not depend only on the

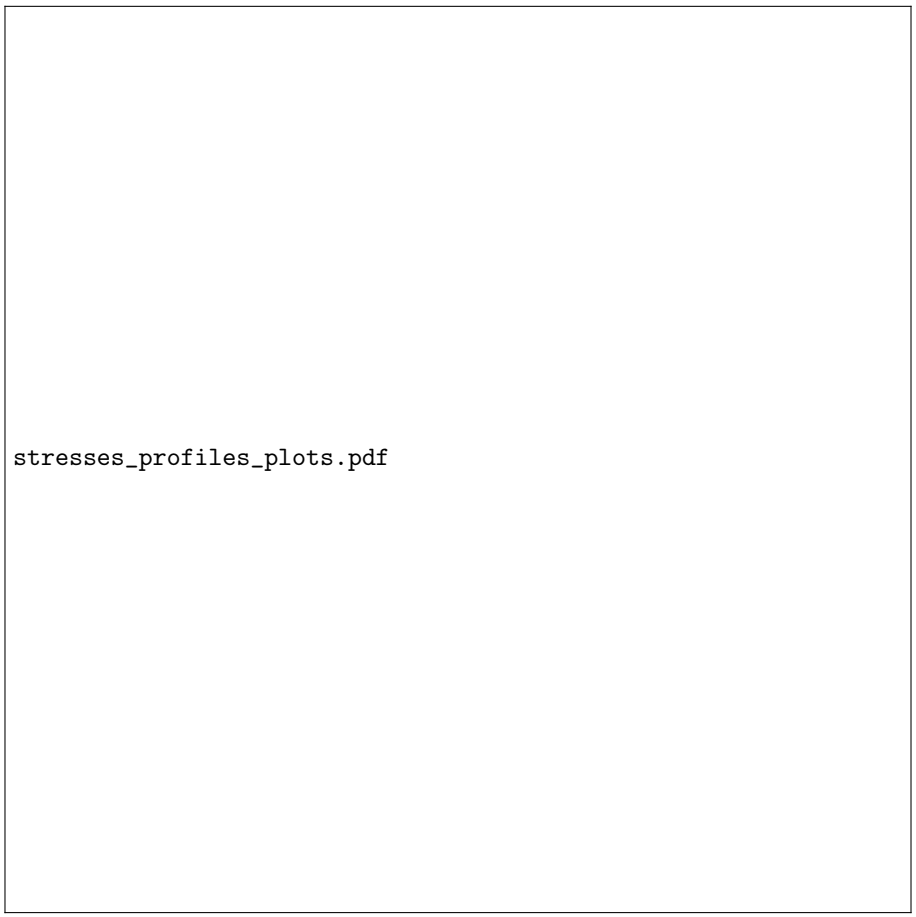

Figure 9: Comparison in terms of longitudinal component of the Piola-Kirchhoff stress tensor $[\mathbf{T}_R]_{33}$ at $X = Z = 0$ within the height of the solid for $\alpha_0 = \{15^o, 45^o, 90^o, 120^o, 180^o\}$ in case of bending model for solid (S), the Euler *Elastica* (EE), nonlinear Euler Elastica (NEE), and finite element (FE): (a) case (I) with $H = B/4$; case (II) with $H = B$; case with (III) $H = 4B$. For each cases $B = 20$ mm and $L = 600$ mm; (d) uniaxial stress-stretch curve of compressible MR material (s vs λ_3 from [**?**]).

geometric aspect ratio of the solid. It will be shown in the following that, for a fixed set of constitutive parameter, the reliability of EE and NEE formulation depends of the Eulerian slenderness β_{ES}.

Results in terms of moment-curvature relation and the associated relative errors ε_r with respect to the FE solution up to $\alpha_0 = 210^o$ are reported in

Figure 10. If the height of the solid is much lower than the length of the

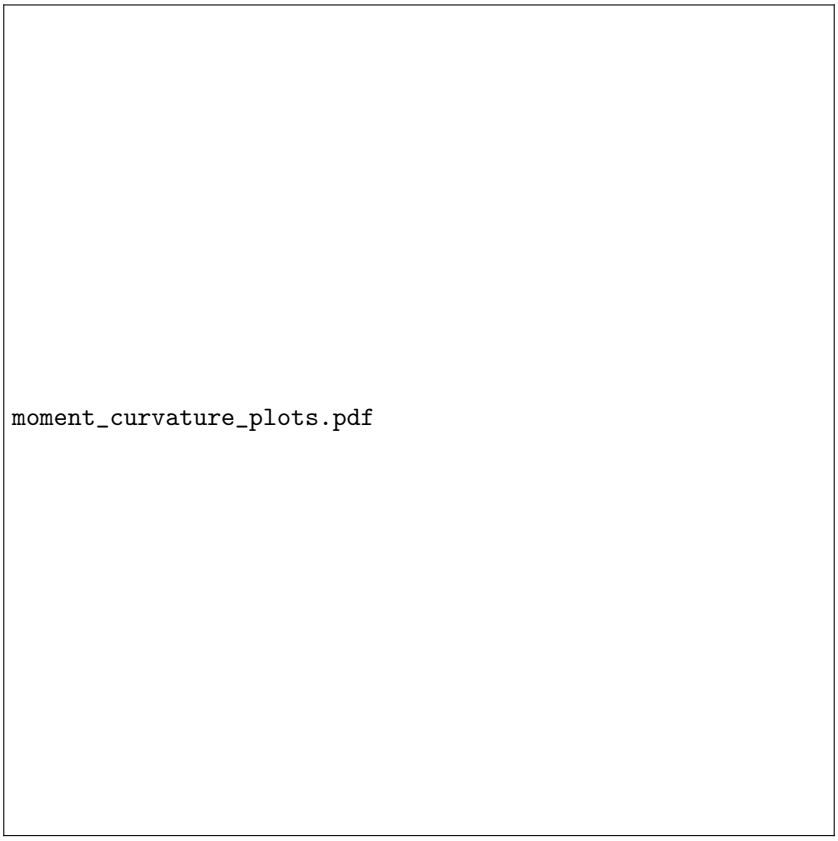

Figure 10: Moment-curvature relations (on left) obtained with model for solid S (black lines), Euler Elastica (red lines), nonlinear Euler Elastica (red dashed lines), FE model (blue lines), and assoicited relative errors (on right) compueted with respect to FE model: (a) case (I) with $H = B/4$; case (II) with $H = B$; case with (III) $H = 4B$. For each cases $B = 20$ mm and $L = 600$ mm.

solid, the moment-curvature relations provide a nearly linear trend for each investigated solution. This happens for cases (I) and (II) as shown in Figs.10(a) and 10(b). Only the EE formulation provides a linear moment-curvature relation (see eq.(36)) regardless of the size of the cross section. Although the moment-curvature relations of the S, NEE and FE models are nonlinear, in cases (I) and (II), they exhibit an almost linear behaviours in the investigated range of

curvature. This is a consequence of the quasi-linear distribution of the stress depicted in Figs.9(a) and 9(b).

When the compactness index β_C is lower than 1 and the Eulerian slenderness β_{ES} is large, as it occurs for cases (I) and (II), the nonlinearities of kinematics and constitutive law are not relevant. For cases (I) and (II), in the investigated range of curvature, all the provided solutions are similar and they are able to grasp the kinematic and, in turn, the global mechanical response of the system. Indeed, the associated relative errors shown in Figs.10(a) and 10(b) are negligible, $\varepsilon_r < 1\%$.

Conversely, If the height of the solid is comparable with the length, moment-curvature relations shows a nonlinear trend for large deformations. It is noteworthy that case (III) exhibits a different behaviour in the moment-curvature response, as depicted in Figure 10(c), in which a softening branch is observed in the solutions provided by S and FE model. On the other hand, the behaviour of the NEE solution shown in Figure 10(c) highlights a slightly hardening response. This behaviour in not correct and differs from both the FE and S predictions. Indeed, the stress profile in Figure 9(c) of case (III) is characterised by an excess of compression that generates a hardening response in terms of moment-curvature law.

As the deformation increases, both the EE and NEE formulations lead to important errors close to 20%, as shown in Figure 10(c). However, the important errors observed in case (III) can also be found in cases (I) and (II) if the Eulerian slenderness decrease. To show that, let introduce the dimensionless bending moment $\overline{m} = m_{\mathrm{S}}/\mathrm{E}_{\mathrm{MR}}BH^2$ [**?**]. The choice of this moment is such to reduce the dimensionless bending moment of the EE formulation (36) to $\overline{m} = \beta_{\mathrm{ES}}^{-1}$.

The dimensionless bending moments of the investigated cases are plotted in Figure 11 as a function of the inverse of the Eulerian slenderness. In such a plot, low values of β_{ES}^{-1} describe cases where the EE formulation, i.e. small deformations and linear elastic constitutive law, can be used to predict stretches and stress resultants. Each investigated case lies on the same curve of Figure 11. The only difference between case (I), (II) and (III) is the value of β_{ES}^{-1} at which

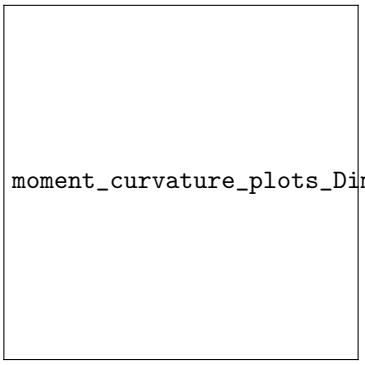

Figure 11: **Introduci il limite della teoria della trave dato in MDPI. Evidenzia l'area tra le due curve**.

that curves are interrupted, corresponding to $\alpha_0 = 210^o$.

In Figure 11, for each case, points corresponding to $\alpha_0 = 210^o$ are denoted with $P_{(I)}$, $P_{(II)}$ and $P_{(III)}$, for case (I), (II) and (III) respectively. For the case (II) (lagrangian high slender solid with compact cross section), if the analysis had investigated curvature values corresponding to $\beta_{\text{ES}}^{-1} = 0.9$, the EE and NEE models would have provided errors in terms of stretch and stress comparable to those of Figs.8(c) and 9(c). For this reason, NUOVA FIGURA AFFIANCO A FIGURA 11, shows the comparison in terms of stress distribution of the case (II), for $\beta_{\text{ES}} = 1.193$. For the case (II), this values, corresponding to $\alpha_0 = 720^o$, provides the same Eulerian slenderness of case (III) at $\alpha_0 = 180^o$. Indeed, as reported by Figure 11(b), the stress exhibits the same behaviour of Figure 9(c) for $\alpha_0 = 180^o$. This confirms that the Eulerian slendernes governs the problem of bending.

Once the constitutive parameter are fixed, the $\overline{m}$ vs β_{ES}^{-1} curve represents the path taken by any solid subject to bending. There are two important aspects that can deviate the behaviour of a 3D solid subject to bending from the curve of Figure 11. Firstly, the onset of local instability phenomena of the cross section not considered in the present kinematic model. Secondly, excessively high $\beta_C = B/H$ ratios in which the transversal kinematic vanishes as a result of plate effects.

In [**?**] for the bending theory of slender beams [**?**], it was already pointed out that there were limits in terms of β_{ES}^{-1} and β_{C} for which that model loses its accuracy. For that model the limit was found in [**?**] corresponding to $\beta_{\mathrm{C}} < 0.5$ and $\beta_{\mathrm{ES}}^{-1} < 0.125$. Those limits are drastically reduced by the present theory of bending. In particular, for the present theory of bent solids, $\beta_{\mathrm{C}} \leq 1/4$ and $\beta_{\mathrm{ES}}^{-1} \leq 1$ ensure relative errors associated to stretches, stresses and bending moment lower than $5\%, 6\%$, and 2% respectively.

The gap between nonlinear trend of case (III) and the linear trend of the Elastica solution in Figure 11, depicted with a grey area, highlights the onset of a nonlinear behaviour (geometrical and constitutive) that take weight as the deformation increases. The growth of this area defines the limitations of the EE theory. For the parameter of the MR material here considered, the limit can be fixed at $\beta_{\mathrm{ES}}^{-1} < 0.5$, corresponding to a relative error in term of bending moment equal to $\varepsilon_r = 5\%$.

7. Conclusions

The problem of finite bending of solids for hyperelastic materials [**?**] has been improved in the present work by considering equilibrium condition in terms of resultant of the normal stress over the cross sections. The relevance of the new obtained equation has been discussed and, in turn, it has been shown that it is fundamental to accurately predict stretch, stress and moment curvature relation of a bent solid for high deformations. Thanks to the new equilibrium equation, the kinematic unknowns of the problem have been properly identified, thus leading to a new moment-curvature relation.

The linearisation of the present model for solids has led to two kinds of approximations. The first one, the Euler *Elastica* (EE) formulation, has been obtained as the leading order term of the series expansion of the kinematics of the present model together with the assumption of a linear constitutive law. Conversely, the linearisation of the kinematics together with the assumption of a nonlinear constitutive law has led to the nonlinear Euler *Elastica* (NEE)

formulation.

The present model of bent solids and its approximations have been compared with 3D FE simulations. Comparisons on three investigated cases, characterised by solids with different heigh of the cross section, have been carried out. Relevant errors, in terms of stretches and stresses distribution within the height of the solid, and bending moment have been found for the case (III) by using the approximated theories. This result is due to the fact that, conversely to cases (I) and (II) in which the solids are extremely slender, in case (III) the solid is characterized by the aspect ratio $B = H/4 = 7.5L$. Thus, it is extremely squat, a non-slender solid. For such a solid, the Eulerian slenderness $\beta_{\rm ES} = R_0/H$ increases faster than the other cases for which the heigh of the solid is lower. However, thanks to the dimensionless form of the moment-curvature relation of present model of bending ($\overline{m}$ vs $\beta_{\rm ES}^{-1}$), it has been discussed how the Euler theories can provide relevant errors also in case of extremely slender solids.

The dimensionless form of the bending moment-curvature relation has been provided in terms of dimensionless bending moment $\overline{m}$ as a function of the inverse of the Eulerian slenderness of the solid $\beta_{\rm ES}^{-1} = H/R_0$. For a fixed values of the constitutive parameters, the $\overline{m}$ vs $\beta_{\rm ES}^{-1}$ relation represents the behaviour of any solids that undergoes bending, infinitesimal or finite bending. For a Mooney-Rivlin material, when the nonlinearities (geometrical and constitutive) take relevance, the $\overline{m}$ vs $\beta_{\rm ES}^{-1}$ curves becomes nonlinear exhibiting softening.

The limits of the present bending theory of solid have been identified corresponding to $\beta_{\rm C} = B/H \leq 1/4$ and $\beta_{\rm ES}^{-1} \leq 1$. These limits are such to ensure relative errors associated to stretches, stresses and bending moment lower than $5\%, 6\%$, and 2% respectively. Under this limits, the relation $\overline{m}$ vs $\beta_{\rm ES}^{-1}$ is independent from the geometries of the solid but, conversely to the Euler Elastica formulation, it is able to predict the nonlinearities in case of large bending. The more the $\overline{m}$ vs $\beta_{\rm ES}^{-1}$ curve differs from linear behavior the more the Elastic Euler formulation fails in the prediction of stretches, stresses, and bending moment.

The curve $\overline{m}$ vs $\beta_{\rm ES}^{-1}$ reveals the limitations of Euler's Elastic theory. The use of such a dimensionless curve can be used to understand until Euler's theory

can be used or, if necessary, it must be substituted or replaced with the theory of the bending of the solid presented here.

8. Acknowledgement

This work was supported by the Italian Ministry of Education, University and Research (MUR) through the PRIN project "Modeling of constitutive laws for traditional and innovative building materials" (code 2017HFPKZY) and through the Project FISR 2019: "EcoEarth" (code 00245).

Appendix A. Relevant kinematic and stress quantities

For convenience, both the main kinematic and stress amounts needed to obtain the relevant expressions reported in the previous Sections are listed in Tables A.1 and A.2.

Appendix B. Relevant loci of the bending model for solids

Four different fundamental neutral loci are considered in the present theory for bending of solids. Each of these geometric loci can be expressed in the reference as well as in the deformed configuration. Neutral loci can be referred to kinematic or mechanical aspects, unstretched or unstressed fibres, respectively. Moreover, neutral loci are associated to longitudinal direction, λ_3 and T_{R_3}, and transversal direction λ and T_{R_1}.

In the reference configuration, the transverse principal stretch λ and longitudinal principal stretch λ_3 are given in eqns.(1) and (2), respectively. The principal stretch λ assumes unitary value at the transverse neutral fibres $N = (0,\, -QN, Z)$, while the principal stretch λ_3 is unitary at the longitudinal neutral fibres $M = (0,\, -QM, Z)$.

The coordinate QN represents a kinematic unknown of the problem. Conversely, QM is obtained as a function of the three kinematic unknowns of the

Kinematics	
Displacement vector, $\mathbf{sp}(P)$	$\begin{bmatrix} \tan\beta\ (r+R-R_0\lambda_3)-X \\ \cos\alpha\ R_0\lambda_3-(R+r-r_{\mathrm{O}})-Y \\ \sin\alpha\ R_0\lambda_3-Z \end{bmatrix}$
Deformation vector, $\boldsymbol{\varphi}(P)$	$\begin{bmatrix} r_{\mathrm{O}}e^{-\frac{Y}{r}}\sin\beta \\ r_{\mathrm{O}}-(r+R)+\left(r+R-r_{\mathrm{O}}e^{-\frac{Y}{r}}\cos\beta\right)\cos\alpha \\ \left(r+R-r_{\mathrm{O}}e^{-\frac{Y}{r}}\cos\beta\right)\sin\alpha \end{bmatrix}$
Transverse (minor) principal stretch, $\lambda(P)$ and $\lambda(P')$	$r_{\mathrm{O}}e^{-\frac{Y}{r}}/r$ $\sqrt{\frac{x^2+\left[r+R-\sqrt{(r+R-r_{\mathrm{O}}+y)^2+z^2}\right]^2}{r^2}}$
Longitudinal (major) principal stretch, $\lambda_3(P)$ and $\lambda_3(P')$	$\left(R+r-r_{\mathrm{O}}e^{-\frac{Y}{r}}\cos\beta\right)/R_0$ $\sqrt{\frac{(r+R-r_{\mathrm{O}}+y)^2+z^2}{R_0^2}}$
Right Cauchy deformation tensor, $\mathbf{C}$	$\begin{bmatrix} \lambda^2 & 0 & 0 \\ 0 & \lambda^2 & 0 \\ 0 & 0 & \lambda_3^2 \end{bmatrix}$
Left Cauchy deformation tensor, $\mathbf{B}$	$\begin{bmatrix} \lambda^2 & 0 & 0 \\ 0 & \lambda^2\cos^2\alpha+\lambda_3^2\sin^2\alpha & \frac{1}{2}\sin 2\alpha\,(\lambda-\lambda_3)^2 \\ 0 & \frac{1}{2}\sin 2\alpha\,(\lambda-\lambda_3)^2 & \lambda^2\sin^2\alpha+\lambda_3^2\cos^2\alpha \end{bmatrix}$
Rotation of XY planes around X, $\alpha(P)$ and $\alpha(P')$	Z/R_0 $\operatorname{atan}\left(\frac{z}{R+y+r-r_{\mathrm{O}}}\right)$
Rotation of ZY planes around Z, $\beta(P)$ and $\beta(P')$	X/r $\operatorname{atan}\left[\frac{x}{R+r-\sqrt{z^2+(R+y+r-r_{\mathrm{O}})^2}}\right]$
Characteristic transversal radii of curvature,	$r_{\mathrm{O}}=r(X,\,0,\,Z)=r\,e^{-\frac{QN}{r}}$, $r_{\min}=r(X,\,H/2,\,Z)=r\,e^{-\frac{H+2QN}{2r}}$, $r_{\max}=r(X,\,-H/2,\,Z)=r\,e^{\frac{H-2QN}{2r}}$
Mapping from Lagrangian to Eulerian coordinates	$\begin{cases} X=-r\,\beta(P') \\ Y=-r\log\{x\csc[\beta(P')]/r\}-QN \\ Z=R_0\,\alpha(P') \end{cases}$

Table A.1: Kinematics of the bending model for solids.

Mechanics	
First Piola-Kirchhoff stress tensor, $\mathbf{T}_R$	$\begin{bmatrix} T_{B_1}\cos\beta & -T_{B_1}\sin\beta & 0 \\ T_{B_1}\cos\alpha\,\sin\beta & T_{B_1}\cos\alpha\,\cos\beta & -T_{B_3}\sin\alpha \\ T_{B_1}\sin\alpha\,\sin\beta & T_{B_1}\cos\beta\,\sin\alpha & T_{B_3}\cos\alpha \end{bmatrix}$
Biot stress tensor, $\mathbf{T}_B$	$\begin{bmatrix} T_{B_1} & 0 & 0 \\ 0 & T_{B_1} & 0 \\ 0 & 0 & T_{B_3} \end{bmatrix}$
Cauchy stress tensor in the principal reference system, $\mathbf{T}$	$\begin{bmatrix} \frac{T_{B_1}}{\lambda\lambda_3} & 0 & 0 \\ 0 & \frac{T_{B_1}}{\lambda\lambda_3} & 0 \\ 0 & 0 & \frac{T_{B_3}}{\lambda^2} \end{bmatrix}$

Table A.2: Mechanics of the bending model for solid.

problem by imposing the unitary value of eq.(12), namely

$$QM = QN + r\log\left(1 + \frac{R - R_0}{r}\right). \tag{B.1}$$

Note that for a MR material (19), eq.(B.1) compared with the constrain $R_0 > R$ given in eq.(26) leads to

$$QN \geq QM \geq 0 \tag{B.2}$$

As a consequence of the kinematic assumptions, in the deformed configuration the unstretched fibres N and M became arcs of circumference characterised by the longitudinal radii of curvature R and R_0, see Figure 2. Indeed, the Eulerian principal stretches assume unitary value at the following characteristic neutral fibres:

$$\begin{aligned} N' &\equiv \left(0,\, r_{\mathrm{O}} - r - R + \sqrt{R^2 - z^2},\, z\right) :\, \lambda(N') = 1 \\ M' &\equiv \left(0,\, r_{\mathrm{O}} - r - R + \sqrt{R_0^2 - z^2},\, z\right) :\, \lambda_3(M') = 1 \end{aligned}. \tag{B.3}$$

In terms of kinematics in the reference configuration, the neutral lines $\mathcal{NL}$ shown in Figure B.12 assume the following form:

$$\begin{aligned} \mathcal{NL}_\lambda &\equiv \left(X,\, -QN,\, 0\right) :\, \lambda(\mathcal{NL}_\lambda) = 1 \\ \mathcal{NL}_{\lambda_3} &\equiv \left(X,\, -QM + r\log\left(\cos X/r\right),\, 0\right) :\, \lambda_3(\mathcal{NL}_{\lambda_3}) = 1 \end{aligned}. \tag{B.4}$$

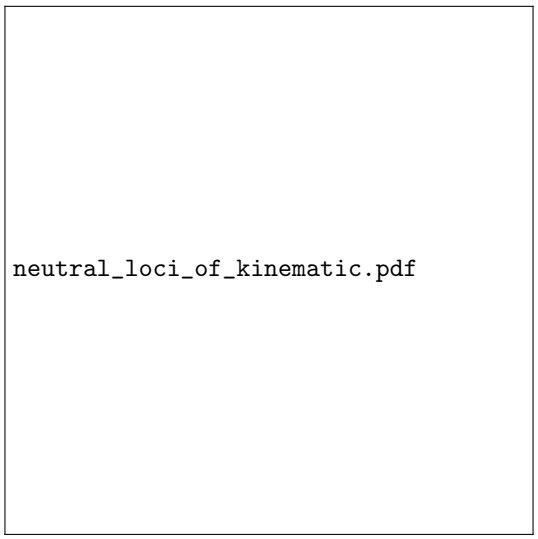

Figure B.12: Kinematic neutral fibres and principal stretch distributions at $X = z = 0$: (a) lagrangian quantities; (b) Eulerian quantities.

Eqns.(B.4) shown that transverse neutral line $\mathcal{NL}_\lambda$ is a straight line parallel to the X axis in the Lagrangian configuration, as shown in Figure B.12. Conversely, Lagrangian longitudinal neutral line $\mathcal{NL}_{\lambda_3}$ varies with the X coordinate assuming a negative concavity.

As a consequence of the longitudinal bending, in the deformed configuration the transversal neutral line $\mathcal{NL}'_\lambda$ assumes a positive concavity, whilst the longitudinal neutral line $\mathcal{NL}'_{\lambda_3}$ becomes a straight line parallel to the X axis, as shown in Figure B.12. This behaviour can be easily proofed recalling eqns.(11) and (12), from which the neutral lines in the deformed configuration read

$$\begin{aligned} \mathcal{NL}'_\lambda &\equiv \left(x,\, r_{\mathrm{O}} - \sqrt{r^2 - x^2},\, 0\right) :\ \lambda(\mathcal{NL}'_\lambda) = 1 \\ \mathcal{NL}'_{\lambda_3} &\equiv \left(x,\, r_{\mathrm{O}} - r + R_0 - R,\, 0\right) :\ \lambda_3(\mathcal{NL}'_{\lambda_3}) = 1 \end{aligned} \quad . \tag{B.5}$$

As shown by relations (B.5), transversal neutral line $\mathcal{NL}'_\lambda$ is an arc of circumference centred at $(x = 0,\, y = r_{\mathrm{O}})$ of radius r whilst longitudinal neutral line $\mathcal{NL}'_{\lambda_3}$ is a straight segment.

The distribution of the 3D neutral loci are here named neutral planes $\mathcal{NP}$.

These loci in reference configuration are defined as

$$\begin{aligned}\mathcal{NP}_\lambda &\equiv \Big(X,\, -QN,\, Z\Big) :\, \lambda(\mathcal{NP}_\lambda) = 1 \\ \mathcal{NP}_{\lambda_3} &\equiv \Big(X,\, -QM + r\log\left(\cos X/r\right),\, Z\Big) :\, \lambda_3(\mathcal{NP}_{\lambda_3}) = 1\end{aligned}, \tag{B.6}$$

Transverse neutral plane $\mathcal{NP}_\lambda$ is a plane parallel to the XZ plane belonging to the coordinate $Y = -QN$. Otherwise, the longitudinal neutral plane $\mathcal{NP}_{\lambda_3}$ is a surface characterized by a negative concavity ($\cos X/r < 1$), Figure B.12.

Based on the mapping between Lagrangian and Eulerian coordinates listed in Table A.1, the neutral planes (B.6) in the deformed configuration turn out to be

$$\begin{aligned}\mathcal{NP}'_\lambda &\equiv \left(x,\, \sqrt{r^2 + (r+R)^2 - x^2 - z^2 + 2(r+R)\sqrt{r^2 - x^2}} + r_{\mathrm{O}} - r - R,\, z\right) :\, \lambda(\mathcal{NP}'_\lambda) = 1, \\ \mathcal{NP}'_{\lambda_3} &\equiv \left(x,\, \sqrt{R_0^2 - z^2} + r_{\mathrm{O}} - r - R,\, z\right) :\, \lambda_3(\mathcal{NP}'_{\lambda_3}) = 1.\end{aligned} \tag{B.7}$$

In relation (B.7)$_1$, the transverse neutral plane $\mathcal{NP}'_\lambda$ represents the equation of the *anticlastic surface* characterised by a saddle-like shape. Differently, the longitudinal neutral plane $\mathcal{NP}'_{\lambda_3}$ is a portion of a cylinder with generating axis directed along the axis X and crossing the coordinate $(y = R_0 + r_O - (r+R), z = 0)$.

The neutral loci in terms of stresses are more complex with respect to those given in terms of stretches because of the dependence on the constitutive model. However, some consideration can be drawn regarding the longitudinal neutral loci of the mechanics in both reference and deformed configurations.

In the reference configuration, the Y coordinates associated to unstressed fibre is obtained by imposing the vanishing of relation (5). Roots of relation (5) provide the unstressed longitudinal neutral fibre $\mathcal{NL}_{T_{B_3}}$ as follow:

$$Y = -QN + r\log\left(\frac{r\cos\beta}{r+R}\right), \quad Y = -QN + r\log\left(\pm\sqrt{-\frac{\sqrt{W_{,2}^2 - W_{,1}W_{,3}} \pm W_{,2}}{W_{,1}}}\right) \tag{B.8}$$

The numerical simulations of the present model of solids suggest that in case of MR material the only admissible root of (B.8) is

$$Y = -QN + \frac{r}{2}\log\left(\frac{W_{,2} - \sqrt{W_{,2}^2 - W_{,1}W_{,3}}}{W_{,1}}\right). \tag{B.9}$$

Therefore, the Lagrangian longitudinal neutral line of the mechanics can be given in the following implicit form:

$$\mathcal{NL}_{T_{B_3}} \equiv \big(X,\, \check{Y}(X),\, 0\big) :\ T_{B_3}(\mathcal{NL}_{T_{B_3}}) = 0, \tag{B.10}$$

in which $\check{Y}(X)$ represents a solution of the following nonlinear equation

$$\check{Y}(X) + QN = r \log \sqrt{\frac{\sqrt{W_{,2}^2 - W_{,1}W_{,3}} - W_{,2}}{W_{,1}}}. \tag{B.11}$$

In particular, for a MR material (19), the Lagrangian longitudinal neutral line (B.11) reads

$$\check{Y}_{\mathrm{MR}}(X) + QN = \frac{r}{2} \log \left(\sqrt{\frac{r^4 R_0^2 e^{\frac{6\check{Y}_{\mathrm{MR}}(X)}{r}}(a+2b+c)}{a r_{\mathrm{O}}^4 \left[r_{\mathrm{O}} - (r+R)e^{\frac{\check{Y}_{\mathrm{MR}}(X)}{r}}\right]^2} - \frac{c}{a} + \frac{b^2}{a^2}} - \frac{b}{a} \right) \tag{B.12}$$

From (B.12) it follows that the longitudinal unstressed fibre shown in Figure B.13(a) for a MR material is assessed as

$$QM_R = \check{Y}_{\mathrm{MR}}(0). \tag{B.13}$$

The position of unstressed fibre (B.13) normalised with respect to the height of the solids is reported in Figure B.13(a) for the cases investigated in Section 6.

From this figure is evident that the position of the unstressed fibre takes relevance as the prescribed rotation α_0 increases. For the case (III) the unstressed fibre plays an extremely important role assuming values closer to 8% of the height of the solid when the solid is bent on itself.

It is also interesting to observe that in case (I), where the base of the solid is higher than the height ($B = 4H = L$), the position of the neutral fibre assumes positive values. However, for the case (I), the distribution of the neutral fibre along the X axis, i.e. the neutral line, changes its sign in the neighbourhood of $B/4$ as reported in Figure B.13. The variation of the neutral line thought-the-width of the solid is much more relevant for case in which $B > H$. This highlight the arising of plate effects. It must be observed that such a variation with respect to X can non be observed by modelling bending using theories based on plane strain regime [**? ? ? ? ?**].

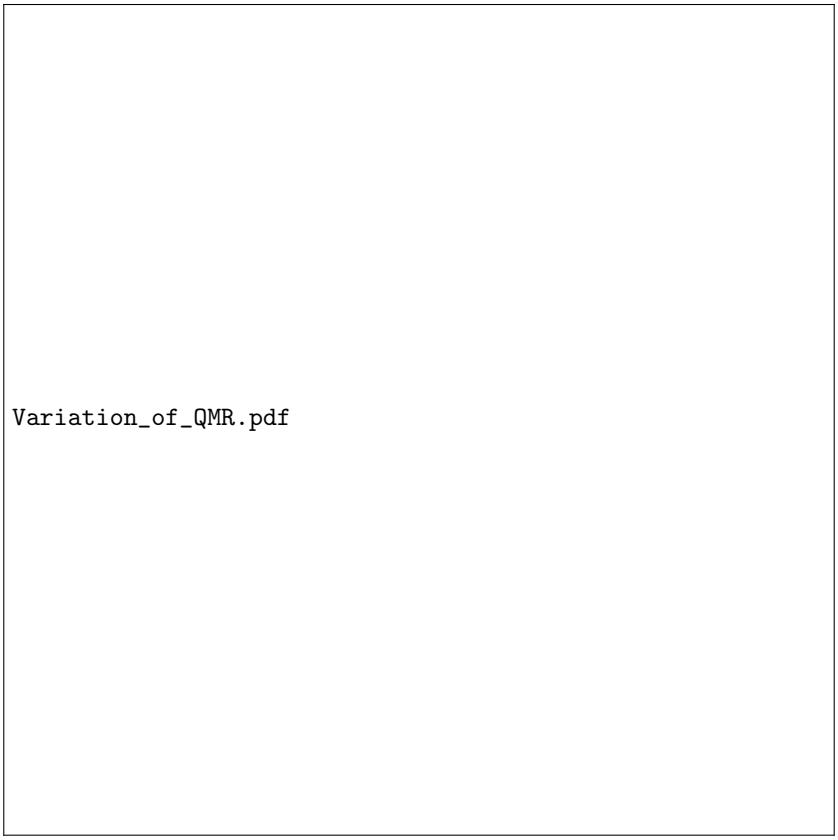

Figure B.13: Effect of the deformation on the longitudinal unstressed geometrical loci: (a) normalised unstressed neutral fibre as a function of its the curvature; (b) distributions of the unstressed neutral line at $\alpha_0 = 180^{\circ}$.

The definition of Cauchy stress component T_3, given in eq.(10), highlights that the Eulerian unstressed longitudinal neutral fibre corresponds with the Lagrangian unstressed longitudinal neutral fibre. Thereby, the Eulerian unstressed longitudinal neutral fibre is assessed by using the deformation component $y(0,\, QM_R,\, 0)$ given in Table A.1, thus leading to

$$QM'_R = r_{\mathrm{O}} \left(1 - e^{-\frac{QM_R}{r}}\right)$$